Available online at www.sciencedirect.com
SCIENCE DIRECT®
Composites Science and Technology 65 (2005) 2407–2415
COMPOSITES SCIENCE AND TECHNOLOGY
www.elsevier.com/locate/compscitech

Modeling of carbon nanotube clamping in tensile tests

Chunyu Li [a], Rodney S. Ruoff [b], Tsu-Wei Chou [a,*]

[a] Department of Mechanical Engineering, University of Delaware, 126 Spencer Laboratory, Newark, DE 19716, USA
[b] Department of Mechanical Engineering, Northwestern University, Evanston, IL 60208, USA

Received 21 June 2005; accepted 22 June 2005
Available online 18 August 2005

Abstract

In this paper, the stress distributions in carbon nanotube clamps such as those formed by the electron beam induced deposition (EBID) technique are analyzed and the contributing factors, including nanotube position, stiffness of clamp material, and thickness of the clamping pad between the AFM tip and the nanotube are examined for the case of tensile loading of the nanotube. The nanotube is modeled at the atomistic scale by the molecular structural mechanics approach and is assumed to be defect free. The clamp material is analyzed by the continuum finite element method. The nanotube and the clamp are assumed to be bonded perfectly to each other. This bonding condition sets the upper limit of clamping capacity. The simulation results indicate that the location and intensity of stress concentration are sensitive to the nanotube orientation. Misaligned nanotubes are likely to break near the edge of the clamp. The clamp material with a lower stiffness (for the stiffness range studied) and a thicker clamping pad between the nanotube and the AFM tip reduce the magnitude of stress concentrations in the clamp.

Keywords: Carbon nanotube; Clamping; Nanocomposites; Multiscale modeling; Tensile testing

1. Introduction

The term 'clamping' here refers to the secure fastening of an already positioned specimen. The sound clamping of a specimen is critical to producing reliable test results of mechanical properties, such as elastic modulus, tensile strength, hardness and fracture toughness. At the macroscopic scale, traditional methods for specimen fastening utilize mechanical, pneumatic or hydraulic clamping [1]. At the microscopic scale, electrostatic and magnetic clamping techniques, for instance, are commonly used for precision machining operations [2,3]. More recently, the development of nanotechnology requires the characterization of properties of nanostructured materials and, hence, the research of nanoscale ultra-precision clamping of specimens [4]. One of the interesting challenges in this regard is the clamping of carbon nanotubes for tensile tests.

Since their discovery, carbon nanotubes offer tremendous opportunity for nanotechnology applications. Examples of their potential applications include as reinforcements for composites [5,6], components of nanoelectromechanical systems [7–9], and storage for hydrogen fuel [10]. Intensive research has been focused on the mechanical and physical properties of carbon nanotubes. Theoretical and experimental studies have confirmed that carbon nanotubes possess extraordinary axial stiffness and tensile strength [11–15]. In these experiments, the appropriate clamping of carbon nanotubes is critical.

There are several suitable methods for attaching a nanotube to a substrate. These include using adhesives such as acrylates, methacrylates or epoxies, employing electrostatic forces, exploiting the chemical affinity between the substrate and the nanotube, and synthesizing

* Corresponding author. Tel.: +1 302 831 1550; fax: +1 302 831 3619.
E-mail address: chou@me.udel.edu (T.-W. Chou).

0266-3538/$ - see front matter © 2005 Elsevier Ltd. All rights reserved.
doi:10.1016/j.compscitech.2005.06.019

the nanotube directly on the substrate. For example, Dai et al. [16] attached carbon nanotubes to an AFM tip with an adhesive. Salvetat et al. [13] and Cuenot et al. [15] attached carbon nanotubes with an atomic force microscope by employing the high surface energy of nanostructures. Yu et al. [14] used the method of electron beam induced deposition (EBID) to clamp carbon nanotubes on AFM tips. Madsen et al. [17] applied EBID to attach nanotubes onto microelectrodes.

The EBID method uses a high-intensity electron beam in an electron microscope. The primary electron beam generates secondary electrons that disassociate residual hydrocarbons in the vicinity of the primary beam spot, leading to the deposition of a hydrogenated amorphous carbon deposit. Recently, Ding et al. [4] reported a rapid method using EBID in an SEM for depositing carbon films in clamping carbon nanotubes. The deposition rate was accelerated by placing a paraffin source of hydrocarbon near the clamp area. The chemical composition, atomic structure, and mechanical properties of such EBID deposits were also investigated in detail [4].

The EBID-based clamping method is rather promising and has motivated us to better understand the fundamental mechanics of such clamps. In this paper, we analyze the stress profiles in the nanotube and its surrounding clamp material as affected by the geometry and elastic properties of the nanotube and the clamp by using a multiscale modeling technique. Potential areas of damage initiation in the clamp have also been investigated.

2. Clamp formed by EBID

Electron beam induced deposition is a process using a high-intensity electron beam, usually within an SEM, to deposit nanoscale structures on a scanned surface. EBID as a technique for serial writing of three-dimensional nanostructures started in the 1980s. Compared with other direct writing technologies using lasers and focused ion beams, EBID has many advantages. These include high spatial resolution, easy control of the beam position, high geometrical flexibility, extremely small feature size, and direct formation of structures from the source materials on a variety of substrates. Using commercially optimized electron-beam systems, EBID has been used to make functional structures, such as sub-10 nm electron gaps [18], nanopores with 1-nm precision [19], nanowires [20], field emission devices [21], thermal sensors [22], and tools for manipulating DNA [23].

Fig. 1 shows a schematic of the EBID process, which can be briefly described as follows. In a vacuum chamber, an electron beam is focused on a substrate surface on which precursor molecules are adsorbed. The precursor molecules may be of any type: organometallic, metal halide, hydrocarbon, etc. As a result of the complex beam induced surface reactions [4, and references therein], the precursor molecules adsorbed in and near to the irradiated area are dissociated and a deposit builds up in the designated location on the substrate.

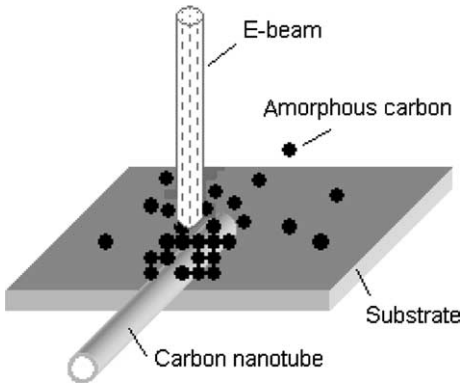

Fig. 1. Schematic illustration of electron beam induced deposition (EBID) on a carbon nanotube.

When used in conjunction with in situ nano-manipulation tools, EBID is capable of forming mechanically strong attachments to carbon nanotubes [14,17]. Yu et al. [14] showed for the first time that solid carbonaceous material could be deposited in an electron microscope onto the surface of an AFM tip as a method of locally clamping a carbon nanotube. The micrograph of Fig. 2 illustrates the clamp formed between an AFM tip and a fiber using EBID. The strength of the clamp is naturally critical to the reliability of the measurements made on the properties of the nanostructured materials. Yu et al. [14] reported that about half of the clamps became detached at the deposition sites during their tensile tests on multiwalled carbon nanotubes. However, the recent work of Ding et al. [4] has demonstrated that larger and consequently much more robust clamps can be rapidly deposited by having a larger con-

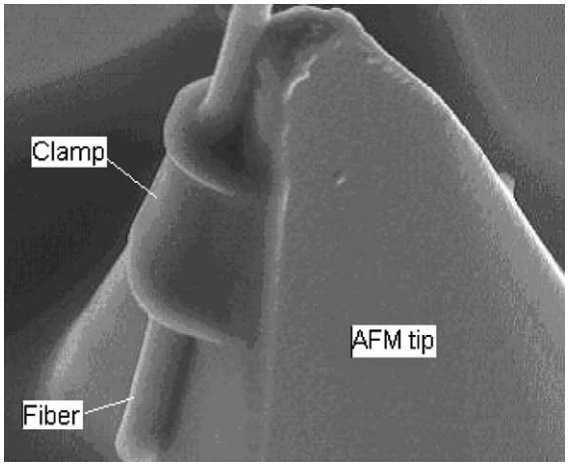

Fig. 2. Clamp formed by EBID [4].

centration of precursor molecules in the deposition zone; in this way failure of the clamp (rather than the specimen) has been dramatically reduced.

3. Modeling of nanotube clamping

The clamping of a carbon nanotube can be modeled as a problem in nanocomposites. Here, the clamp material is treated as the matrix material that surrounds the carbon nanotube, or the reinforcement phase. The only difference between a nanotube clamp and a traditional composite is that, instead of being totally embedded in the matrix, the carbon nanotube protrudes from the clamp material. Thus, the tensile load applied by the AFM tip is transferred to the carbon nanotube through its bonding with the clamp (matrix) material.

Consequently, the modeling of the nanotube clamping can be performed following the same procedure as that used for simulating carbon nanotube-reinforced composites [24]. In this study, only the clamping of a single-walled carbon nanotube is considered.

3.1. Modeling of carbon nanotubes

The modeling of nanotubes is conducted at the atomistic scale. The molecular structural mechanics approach [25], which has been successfully used for studying static, dynamic and thermal properties of carbon nanotubes [7,9,26–29], is adopted for modeling of the nanotubes. The main concept of this approach is briefly outlined below.

In the molecular structural mechanics method, a single-walled carbon nanotube is simulated as a space frame structure, where the covalent bonds in the nanotube are treated as connecting beams and the carbon atoms as joint nodes in the frame structure. If the equivalent beam is assumed to be of round cross-section, only three stiffness parameters, i.e., the tensile resistance EA, the flexural rigidity EI, and the torsional stiffness GJ, need to be determined for the analysis. Here, E and G are, respectively, the Young's modulus and shear modulus of the beam, A, I and J are, respectively, the area, the moment of inertia and the polar inertia of the beam cross-section. Then, the concept of energy equivalence between local potential energies in computational chemistry and elemental strain energies in structural mechanics is adopted. A figure schematically showing the energy equivalence between atomic bonds and their equivalent beams can be found in [25], and a direct relationship between the structural mechanics parameters and the molecular mechanics force field constants is established, i.e.,

$$\frac{EA}{L} = k_r, \quad \frac{EI}{L} = k_\theta, \quad \frac{GJ}{L} = k_\tau, \tag{1}$$

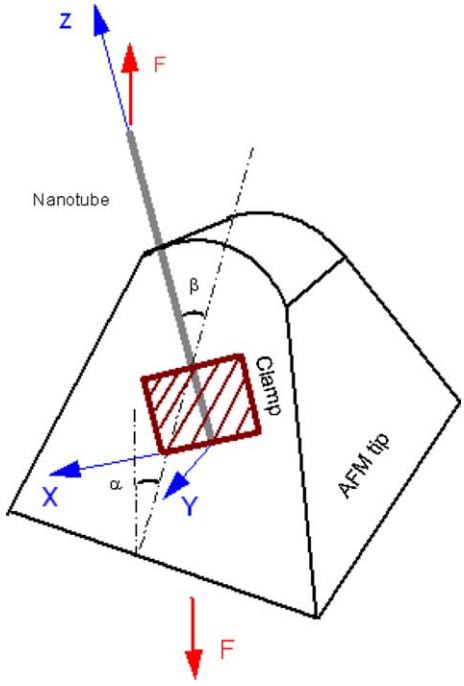

Fig. 3. Nanotube position on the surface of AFM tip.

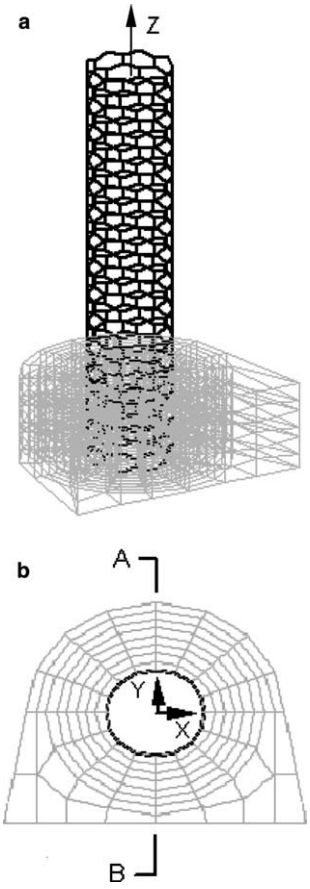

Fig. 4. Simulation model of nanotube clamp: (a) side view and (b) top view.

where k_r, k_θ and k_τ are the force field constants in molecular mechanics. Then, following the procedure of the structural mechanics technique, the nanotube deformation under certain loading conditions can be readily solved.

3.2. Modeling of clamp materials

According to Ding et al. [4], the typical deposit formed by EBID using *n*-Docosane ($C_{22}H_{46}$) and perdeuterated *n*-Tetracosane ($C_{24}D_{50}$) precursor sources is hydrogenated amorphous carbon (a-C:H). The Young's modulus was fit as 34 GPa from nanoindentation experiments [4]. This value is much lower than those obtained from computer simulations by Tersoff [30], which are in the range of 100–700 GPa and decrease with increasing hydrogen content. The difference in Young's modulus values stems from the fact that the computer simulations assumed a hydrogenated amorphous carbon with nearly ideal sp^3 bonding while the deposited hydrogenated amorphous carbon in Ref. [4] has significantly more sp^2- than sp^3-bonded carbon.

Since the computational task of simulating the clamp material using atomistic modeling alone is formidable, it is treated as a continuum in the present analysis and the finite element method is adopted for analyzing its deformation. The cubic isoparametric elements are used in the meshing of the clamp material. By taking into account the range of both experimental and theoretical values in the literature, we use the Young's modulus values of 34, 100 and 300 GPa in our simulations to address the effect of clamp material stiffness on clamping capacity.

3.3. Modeling of nanotube/clamp interface

Because the nanotube is modeled at the atomistic scale and the clamp material is treated as a continuum, the modeling of the nanotube/matrix interface requires additional assumptions. In this paper, we consider the carbon nanotube and the clamp material to be perfectly

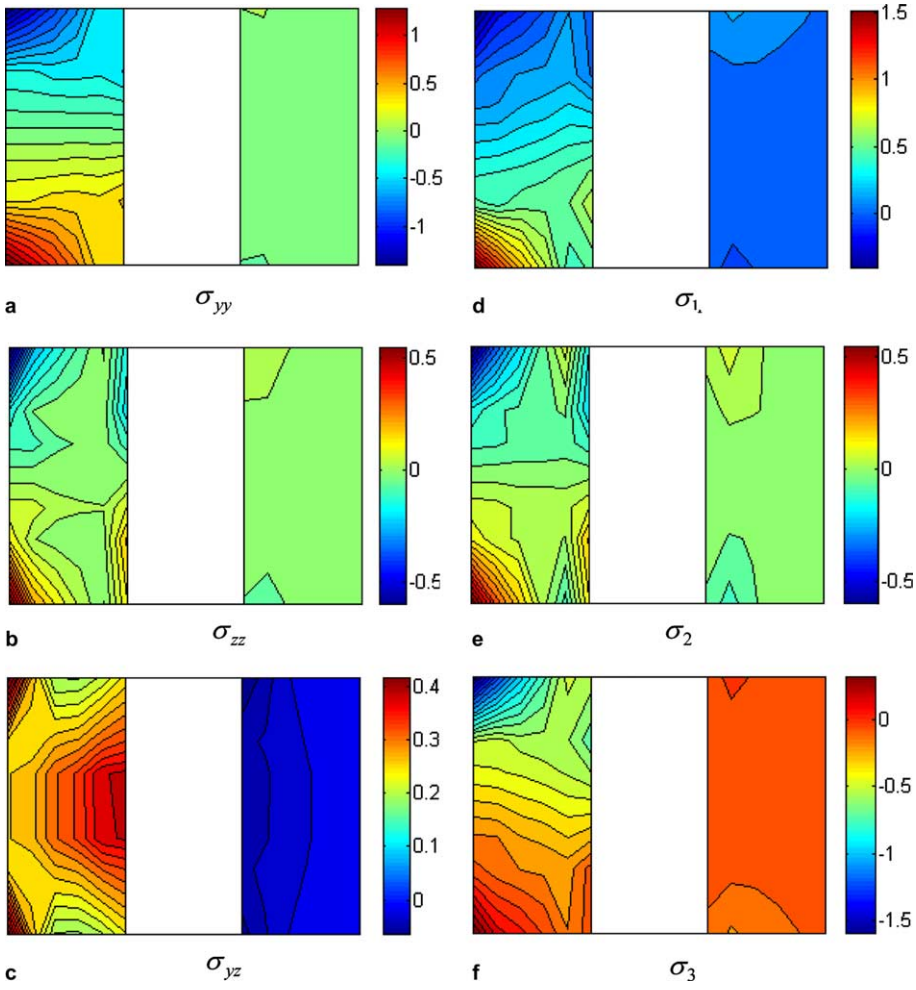

Fig. 5. Stress distribution in the clamp material for the ideal nanotube position of $\alpha = \beta = 0°$ (the left side depicts the part of clamp between the AFM tip and the nanotube, and the central region is the section of the nanotube).

bonded at the interface. This assumption leads to the highest interfacial load transfer efficiency and, hence, the upper bound in tensile load capacity.

For the perfectly bonded interface, it is assumed that the outer surface of the nanotube coincides with the inner cylindrical surface of the clamp material. In order to match the atoms in the nanotube and the nodes in the finite elements, the center of the atom in the nanotube is assumed to be located on the outer surface, not in the center of the tube wall. Because the elastic stiffness of carbon nanotubes is not strongly dependent on nanotube diameter [25], this position shift would not significantly affect the modeling results of nanotube deformation. Also, the corner nodes of finite elements in the clamp material are assumed to coincide with atoms in the nanotube.

4. Results and discussion

In this paper, the focus of the analysis is on the elastic interaction between a nanotube and its surrounding clamp material, which is deposited on an AFM tip. The nanotube, which is anchored at the other end by a similar clamp to an opposing AFM cantilever tip, is stretched in tension. Fig. 3 shows schematically the position of a carbon nanotube clamped on the AFM tip. The AFM tip surface is inclined at the angle α from the vertical line, along which the axial force is applied. The nanotube is assumed to lie in the inclined surface. The angle between the tube axis and the centerline of the inclined surface is denoted as β, which may be present during clamp deposition. The coordinate system is centered at the clamped end of the tube, the Z-axis coincides with the axial direction of the nanotube and the X–Z plane is parallel to the inclined AFM tip surface. The AFM tip is assumed to be a rigid solid and the perfect bonding condition mentioned above is imposed on the interface between the clamp and the AFM tip. The total force exerted by the AFM tip in pulling the nanotube is denoted by F, which is assumed to be in the direction normal to the base plane of the AFM tip. Thus, the axial force in the nanotube is $F_z = F\cos\alpha\cos\beta$. Also, there are force components in transverse directions, i.e., $F_x = F\cos\alpha\sin\beta$ and $F_y = F\sin\alpha$. It is understood that, depending upon the geometry of the AFM tip and the way the nanotube is clamped, the resultant force F acting on the base of the AFM tip and the vertical force F associated with the nanotube may not be coaxial. As a

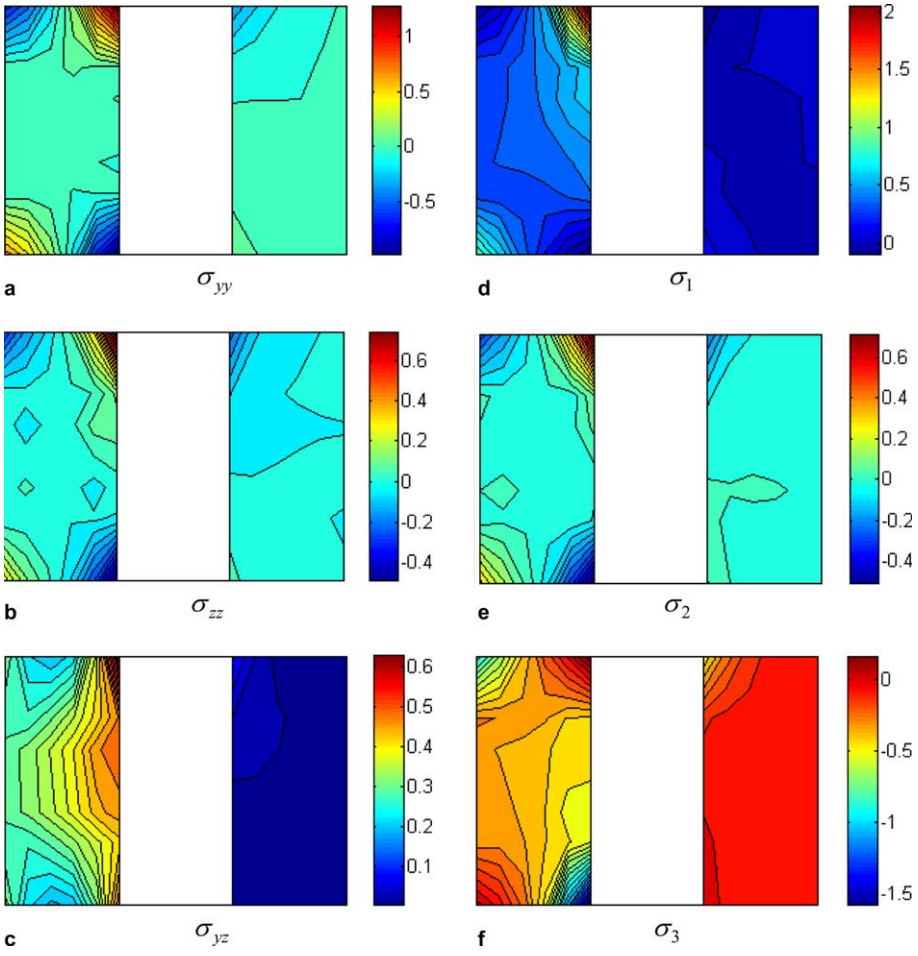

Fig. 6. Stress distribution in the clamp material for misaligned nanotube orientation, $\alpha = \beta = 5°$.

result, a moment is induced in the nanotube, which increases in magnitude with distance from the clamp.

According to the maximum normal stress criterion, failure occurs whenever the largest principal stress reaches the material failure strength. The principal stresses can be obtained from the general stress tensor by solving the eigenvalue equation. Thus, in our investigation of the stress distribution in the clamp material, the focus is on the location of maximum stress concentration, as well as the effects of various contributing factors, such as the stiffness of clamp material, clamp thickness, and nanotube inclination angles.

Fig. 4 displays the computational model for the clamp. In the simulations, the Young's modulus of the clamp material is assumed to be 34 GPa unless stated otherwise and the Poisson's ratio of the clamp material is assumed to be 0.3. Other basic parameters are: nanotube length 6.25 nm (Fig. 4(a)), nanotube (8, 0) diameter 0.63 nm, clamp height 1.14 nm (Fig. 4(a)), and the thickness of clamp material coverage on the side opposite to the nanotube/AFM tip interface is 0.64 nm (Fig. 4(b)). The stresses are normalized by the applied force F (nN) and thus the unit of stresses in the figures is nm^{-2}. The profiles of stress distribution shown in Figs. 5–8 are the stresses at the cross-section AB of the clamp. Thus, in each figure, the center region is the section of the nanotube; the left side depicts the part of clamp between the AFM tip and the nanotube; and the right side is the part of clamp covering the nanotube.

First, we consider the case where the nanotube is assumed to be in an ideal position, i.e., $\alpha = \beta = 0°$. Fig. 5 shows the distributions of axial, transverse, and shear stresses σ_{zz}, σ_{yy}, and σ_{yz}, respectively, as well as principal stresses in three directions. It can be seen that the stress distribution is rather complicated. Stress concentrations occur at the lower and upper corner near the AFM tip, and both σ_{zz} and σ_{yy} are in tension at the lower corner and compression at the upper corner. The stress σ_{yz} appears to be symmetric with respect to the mid-section in the thickness direction of the clamp. The maximum values of all three principal stresses occur at the lower corner near the AFM tip, which is the potential area of damage initiation in the clamp.

Fig. 6 shows the stress distributions in the clamp material for $\alpha = \beta = 5°$, namely, the nanotube is not in an ideal orientation and it is forming two non-zero

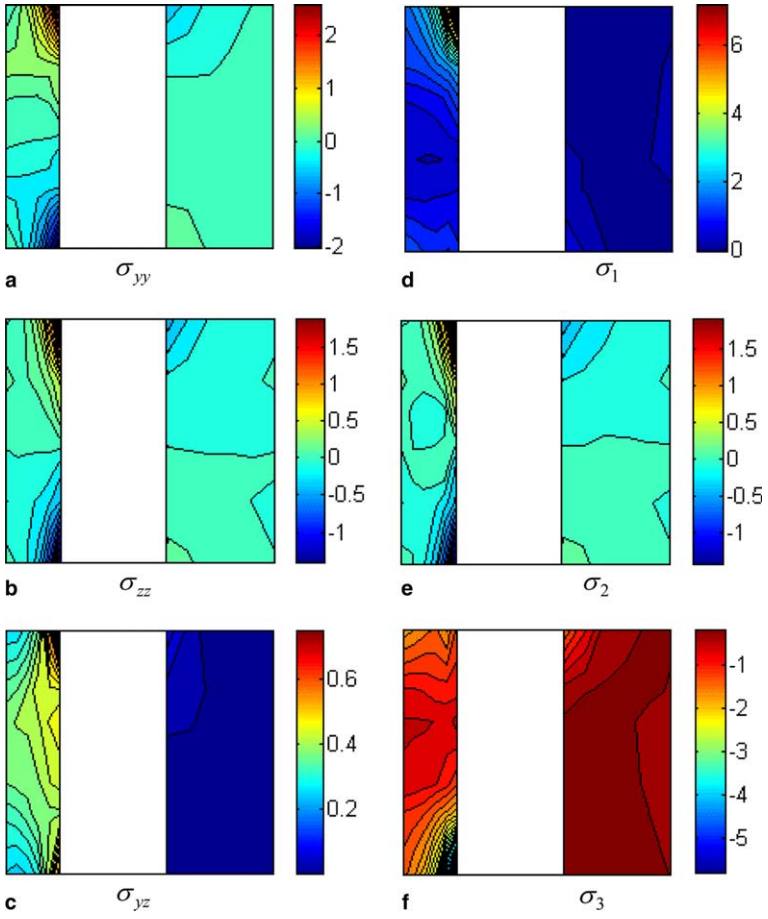

Fig. 7. Stress distribution in the clamp material for misaligned nanotube orientation, $\alpha = 5°$, $\beta = 30°$.

angles with the applied force F. The most significant difference between the stress distributions of this misaligned case and the well-aligned case (Fig. 5) is that the stress concentrations also occur at the clamp/nanotube interfacial area. The anti-symmetric distribution of σ_{yy} and σ_{zz} through the thickness of the clamp materials between the clamp/AFM tip and clamp/nanotube interfaces reflects the bending and torsion induced by the misalignment. The magnitudes of principal stress are also higher than those in Fig. 5.

Sometimes, there is a much larger misalignment between the loading direction and the axial direction of the carbon nanotube. The stress concentrations are expected to be more serious as misalignment increases. Fig. 7 shows the stress distributions in the clamp material for $\alpha = 5°$ and $\beta = 30°$. The distributions of σ_{yy} and σ_{zz} through the thickness of the clamp materials between the clamp/AFM tip and clamp/nanotube interfaces are no longer anti-symmetric and the stress concentrations at the clamp/nanotube interface are significantly higher. The magnitude of maximum principal stress is more than three times of that in Fig. 6. Thus, the effect of misalignment on the clamping capacity is significant.

Fig. 8 displays the distributions of maximum principal stress in the clamp material for three different Young's modulus values: (a) 34 GPa; (b) 100 GPa; and (c) 300 GPa. The inclination angles are taken as $\alpha = 5°$ and $\beta = 0°$. The results indicate that the contours of maximum principal stress are roughly the same for the three cases, but the magnitude of maximum stress increases slightly with increasing clamp material stiffness. As shown in the figure, the maximum tensile stress

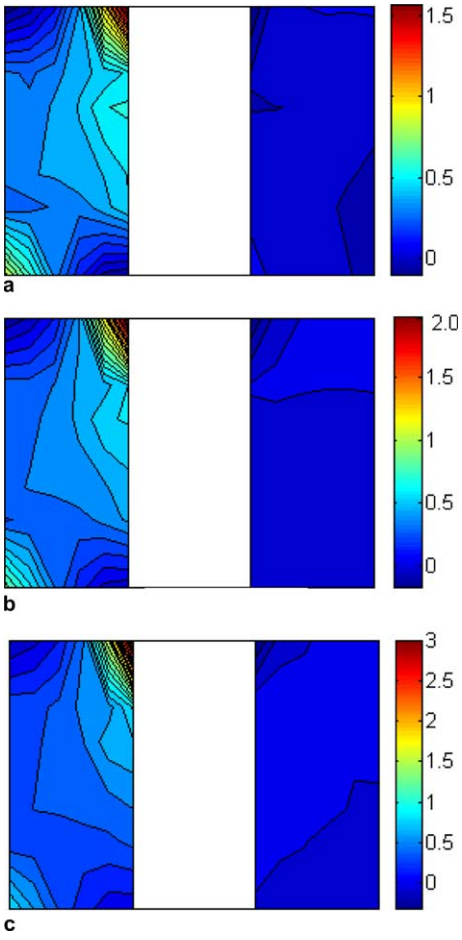

Fig. 8. Distributions of maximum principal stress in the clamp material having different Young's modulus: (a) 34 GPa; (b) 100 GPa; (c) 300 GPa.

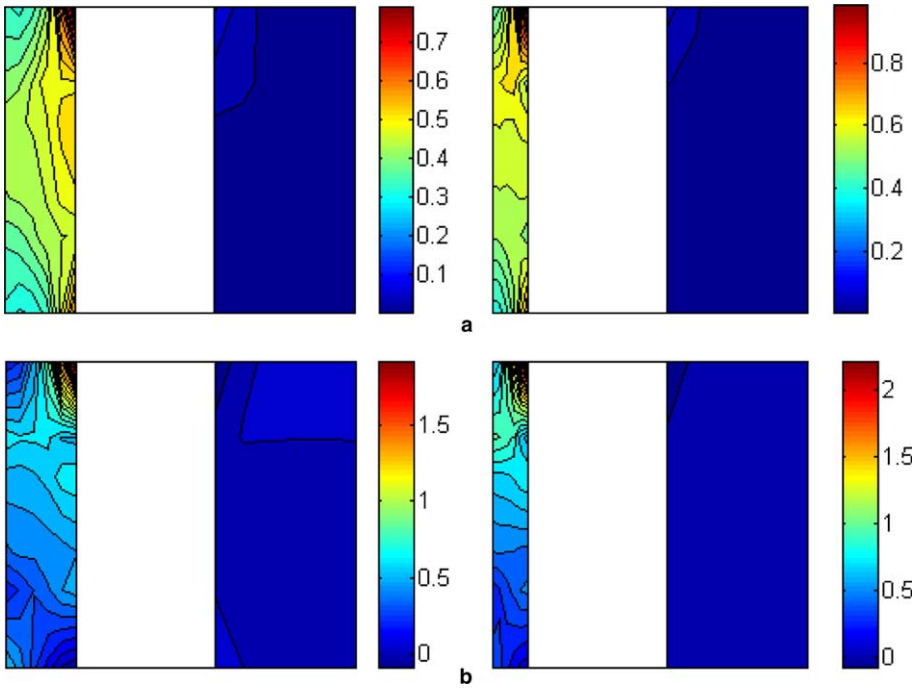

Fig. 9. Effect of clamp pad thickness on the distribution of stress: (a) shear stresses and (b) maximum principal stress.

appears at the nanotube/clamp interface. Since the clamp material is basically hydrogenated amorphous carbon the interfacial bonding strength may not be significantly affected by the stiffness of the clamp material. Therefore, the less stiff clamp material may be more desirable for reducing the stress concentration, and, hence, interfacial tensile failure.

The thickness of clamp material between the nanotube and the AFM tip has a significant effect on the stress distributions. We refer to this part of the clamp material as the "clamping pad". Fig. 9 shows the thickness effect of the clamping pad on the shear stress σ_{yz} and the maximum principal stress. It is seen that the stresses increase with decreasing thickness of the clamping pad. The maximum shear stress is increased approximately by 25% if the thickness is reduced to one half. This means that a thicker clamping pad is more desirable for reducing the chance of interfacial failure.

In the experiments reported by Yu et al. [14] for measuring the tensile strength of carbon nanotubes, there were 21 cases of clamp failure and 19 of nanotube fracture within the gauge length. Having confirmed the magnitude of stress concentrations that may be responsible for clamp failure from the above modeling analysis, it is also essential to investigate the stress distribution in the nanotube to gain a better understanding of how and where a nanotube will break. Fig. 10 illustrates the computational results for axial stress distribution along the carbon nanotube normalized by the applied stress. Four different cases are considered, i.e., (a) $\alpha = \beta = 0°$; (b) $\alpha = 5°$, $\beta = 0°$; (c) $\alpha = \beta = 5°$ and (d) $\alpha = 5°$, $\beta = 30°$ and the nanotube length is 6.25 nm. For case (a), the axial stress is uniformly distributed along the nanotube length in the part not covered by the clamp. But for cases (b), (c) and (d), the axial stresses in the nanotube have a significant magnification in the region near the edge of the clamp. This stress magnification is due to the bending and torsional moments resulted from the misalignment of nanotube with the tensile load. Thus, it can be concluded that nanotube breaking will mostly occur near the edge of the clamp if the nanotube is not well aligned with the direction of applied force. This finding is consistent with the experimental observations for solid nanowires tested recently in the Ruoff group, such as boron and carbonized electrospun PAN-based nanofibers. We note that even though there was misalignment in the work of Yu et al. [14], failure in the 19 successful tests occurred at essentially random locations along the outer shell of the MWCNTs. The range of fracture strengths, relative to the expected fracture strength of a defect free carbon nanotube, has been rationalized as due to the presence of large "holes" in the outer shell from oxidative pitting [31,32].

It should be noted that our analysis focuses on a few key factors which influence the clamping capacity and

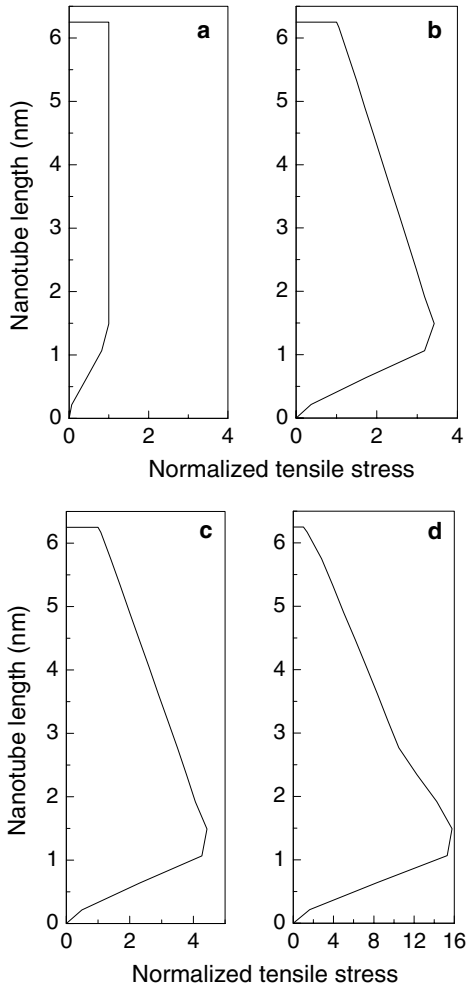

Fig. 10. Maximum axial stresses along the nanotube length for: (a) $\alpha = \beta = 0°$; (b) $\alpha = 5°$, $\beta = 0°$; (c) $\alpha = \beta = 5°$; (d) $\alpha = 5°$, $\beta = 30°$.

nanotube failure. By assuming a rigid AFM tip, the analysis does not take into account its deformation. Practically, the AFM tip made of silicon has a Young's modulus about 150 GPa. Sometimes, there is a thin layer of SiO_2 on the silicon tip and the Young's modulus is even lower (roughly 60–70 GPa). Therefore, the magnitudes of the stiffnesses of the clamp material and the AFM tip are in the same order. If the deformation of the AFM tip were included for more accurate analysis, the stress concentrations at the interface between the AFM tip and the clamp material would be less than the present results. However, our simulations indicate that the most serious stress concentration usually occurs at the clamp/nanotube interface, due to the inevitable misalignment in experiments between the load direction and the axial direction of nanotube.

5. Conclusions

The proper clamping of a carbon nanotube to the tip of an AFM determines the effectiveness in nanotube

tensile testing. In this paper, we analyze the stress distribution of nanotube clamps formed by the EBID technique and examine the contributing factors, including nanotube position, stiffness of clamp material, and thickness of the clamping pad between the AFM tip and the nanotube. The numerical analysis is performed by a multiscale modeling technique. The nanotube is modeled at the atomistic scale by the molecular structural mechanics approach, and the clamp material is analyzed by the continuum finite element method. The nanotube and the clamp material are assumed to be perfectly bonded. The simulation results indicate that the location and intensity of stress concentration are sensitive to the nanotube orientation. The clamp material with a relatively lower stiffness reduces the magnitude of stress concentration. Also, the increase of the thickness of the clamping pad between a nanotube and the AFM tip reduces the tensile stress concentration. The misalignment between the applied tensile force and the nanotube orientation results in bending and torsional loads on the nanotube and, hence, additional interfacial shear stress concentrations in the clamp material. Also, the misalignment is in part responsible for having caused failure of carbon nanotubes near the edge of the clamp.

Acknowledgements

This work is supported by the National Science Foundation (NIRT Program, Grant No. 0304506, Dr. Ken P. Chong, Program Director) and the Army Research Office (Grant No. DAAD 19-02-1-0264, Dr. Bruce LaMattina, Program Director).

References

[1] Raabe J. Hydro power: the design, use, and function of hydromechanical, hydraulic, and electrical equipment. VDI-Verlag; 1985.
[2] Kalkowski G, Risse S, Harnisch G, Guyenot V. Electrostatic chucks for lithography applications. Microelectron Eng 2001;57:219–22.
[3] De Stefani JD. Magnetic Chucks Attract New User. Tool Product 1994;60:61–4.
[4] Ding W, Dikin DA, Chen X, Wang X, Li X, Piner RD, et al. Clamping nano-structures using electron beam induced deposition. J Appl Phys 2005;98:014905.
[5] Thostenson ET, Ren Z, Chou TW. Advances in the science and technology of carbon nanotubes and their composites: a review. Compos Sci Technol 2001;61:1899–912.
[6] Thostenson ET, Li CY, Chou TW. Nanocomposites in context. Compos Sci Technol 2005;65:491–516.
[7] Li CY, Chou TW. Single-walled carbon nanotubes as ultrahigh frequency nanomechanical resonators. Phys Rev B 2003;68:073405.
[8] Li CY, Chou TW. Mass detection using carbon nanotube-based nanomechanical resonators. Appl Phys Lett 2004;84:5246–8.
[9] Li CY, Chou TW. Strain and pressure sensing using single-walled carbon nanotubes. Nanotechnology 2004;15:1493–6.
[10] Darkrim FL, Malbrunot P, Tartaglia GP. Review of hydrogen storage by adsorption in carbon nanotubes. Int J Hydrogen Energy 2002;27:193–202.
[11] Treacy MMJ, Ebbesen TW, Gibson TM. Exceptionally High Young's modulus observed for individual carbon nanotubes. Nature 1996;381:680–7.
[12] Wong EW, Sheehan PE, Lieber CM. Nanobeam mechanics: elasticity, strength, and toughness of nanorods and nanotubes. Science 1997;277:1971–5.
[13] Salvetat JP, Bonard JM, Thomson NH, et al. Mechanical properties of carbon nanotubes. J Appl Phys A 1999;69:255–60.
[14] Yu MF, Lourie O, Dyer MJ, Moloni K, Kelly TF, Ruoff RS. Strength and breaking mechanism of multi-walled carbon nanotubes under tensile load. Science 2000;287:637–40.
[15] Cuenot S, Demoustier-Champagne S, Nysten B. Elastic modulus of polypyrrole nanotubes. Phys Rev Lett 2000;85:1690–3.
[16] Dai HJ, Hafner JH, Rinzler AG, Colbert DT, Smalley RE. Nanotubes as nanoprobes in scanning probe microscopy. Nature 1996;384:147–50.
[17] Madsen DN, Molhave K, Mateiu R, Rasmussen AM, Brorson M, Jacobsen CJH, et al. Soldering of nanotubes onto microelectrodes. Nano Lett 2003;3:47–9.
[18] Liu K, Avouris P, Bucchignano J, Martel R, Sun S, Michl J. Simple fabrication scheme for sub-10 nm electrode gaps using electron-beam lithography. Appl Phys Lett 2002;80:865–7.
[19] Storm AJ, Chen JH, Ling XS, Zandbergen HW, Dekker C. Fabrication of solid-state nanopores with single-nanometre precision. Nature Mater 2003;2:537–40.
[20] Silvis-Cividjian N, Hagen CW, Kruit P, VanderStam MAJ, Groen HB. Direct fabrication of nanowires in an electron microscope. Appl Phys Lett 2003;82:3514–6.
[21] Dong LX, Arai F, Fukuda T. Electron-beam-induced deposition with carbon nanotube emitters. Appl Phys Lett 2002;81:1919–21.
[22] Mailly F, Giani A, Bonnot R, Temple-Boyer P, Pascal-Delannoy F, Foucaran A, et al. Anemometer with hot platinum thin film. Sensors Actuat A 2001;94:32–8.
[23] Baba M, Sano T, Iguchi N, Iida K, Sakamoto T, Kawaura H. DNA size separation using artificially nanostructured matrix. Appl Phys Lett 2003;83:1468–70.
[24] Li CY, Chou TW. Multiscale modeling of carbon nanotube reinforced polymer composites. J Nanosci Nanotechnol 2003;3:423–30.
[25] Li CY, Chou TW. A structural mechanics approach for the analysis of carbon nanotubes. Int J Solids Struct 2003;40:2487–99.
[26] Li CY, Chou TW. Elastic properties of single-walled carbon nanotubes in transverse directions. Phys Rev B 2004;69:073401.
[27] Li CY, Chou TW. Vibrational behaviors of multi-walled carbon nanotube-based nanomechancial resonators. Appl Phys Lett 2004;84(1):121–3 (SCI 759BH).
[28] Li CY, Chou TW. Quantized molecular structural mechanics modeling for specific heat of single-walled carbon nanotubes. Phys Rev B 2005;71:075409.
[29] Li CY, Chou TW. Axial and radial thermal expansion of single-walled carbon nanotubes. Phys Rev B 2005;71:235414.
[30] Tersoff J. Structural properties of sp^3-bonded hydrogenated amorphous carbon. Phys Rev B 1991;44:12039–42.
[31] Mielke SL, Troya D, Zhang S, Li JL, Xiao SP, Car R, et al. The role of vacancy defects and holes in the fracture of carbon nanotubes. Chem Phys Lett 2004;390:413–20.
[32] Pugno NM, Ruoff RS. Quantized fracture mechanics. Philos Mag 2004;84:2829–45.